Synthesis of Mesoporous NiFe2O4 Nanoparticles for Enhanced Supercapacitive Performance

Nagesh Kumar, Amit Kumar, Sridhar Chandrasekaran, and Tseung Yuen Tseng

***Abstract*—In this study a simple one step hydrothermal method has been utilized to synthesize mesoporous $NiFe_2O_4$ nanoparticles. The prepared $NiFe_2O_4$ (NFO) is highly crystalline and possesses homogenously distributed mesopore. The structural analysis, thermal stability and morphological studies of mesoporous NFO nanoparticles are performed using XRD, TGA, TEM, FE-SEM and surface area analyzer. The supercapacitive behavior of synthesized nanomaterial is investigated in a three-electrode configuration cell with 2 M KOH electrolyte using cyclic voltammetry, galvanostatic charge-discharge cycling and electrochemical impedance spectroscopy. The mesoporous crystalline NFO nanoparticles (diameter 10-15 nm) intuitively possess interesting structural advantages, such as high surface area (148 $m^2.g^{-1}$), fast electron and ion transport. As a result, it exhibits very good specific capacitance (1040 $F.g^{-1}$ at 1 $A.g^{-1}$) and good cycling stability (~70 % up to 500 cycles at 2 $A.g^{-1}$) when examined as electrode material for high performance electrochemical supercapacitor applications.**

***Index Terms*—Mesoporous, $NiFe_2O_4$, Nano particles, Supercapacitor.**

I. Introduction

In response to the ever-growing concerns for environmental issues like global warming and increasing thirst for energy, the renewable energy resources like solar, wind and hydro energy have become prime focus of the major world powers and scientific research community [1]. In order to maximum utilization of renewable energy resources and to get abiding energy supply, these must be connected to some appropriate energy storage devices like batteries, fuel cells and supercapacitors (SCs) [2]. Among these energy storage devices, SCs, also known as electrochemical capacitors or ultracapacitors, have attracted much attention due to their excellent power density (>10 kW kg^{-1}) and long cycle life (>10^5 cycles) and fast galvanostatic charge discharge (GCD) response (within seconds) [3]-[6]. But, the poor energy density of SCs is the main issue, which limits their propitious industrial utilization. Therefore, a lot of scientific endeavor is going on to improve the overall performance of SCs. Depending on their charge storage mechanism, the SCs have been divided into two main categories, namely electric double layer supercapacitors (EDLSCs) and pseudocapacitors or faradaic supercapacitors (FSCs). In EDLSCs, the charge storage mechanism is governed by ions absorption/desorption process at the electrode-electrolyte interface, while in pseudocapacitors reversible redox reactions on the surface of the active material store the charges. Generally, carbon-based materials (CNT, graphene and mesoporous carbon) are used as active electrode materials for designing the EDLSCs, and on the other hand, the active electrode materials for FSCs are metal oxides and conductive polymers. In comparison to EDLSCs, generally, FSCs exhibit higher specific capacitance and hence superior energy density [7], [8]. Keeping this in mind, various metal oxides, such as NiO, RuO_2, MnO_2, Co_3O_4, V_2O_5 and Fe_3O_4 with enhanced specific surface area and suitable pore size have been prepared using different synthesis methods [9]-[14]. Recently, the electrochemical properties of different spinel mixed metal oxides, such as $MnCo_2O_4$, $NiCo_2O_4$, $CoMoO_4$, $CoFe_2O_4$, $NiMn_2O_4$, $NiFe_2O_4$, and $ZnMn_2O_4$ have been studied due to their good electrical conductivity, low cost, good structure stability and relatively high specific capacitance [15]-[21]. Here, it has concluded that the electrochemical performance of such systems can be tuned effectively by their morphology, surface area and pore size distribution. Among spinal Ni ferrite, magnetite and cobaltite, the electrochemical properties of various Ni cobaltite ($NiCo_2O_4$) morphological structures such as tremella-like, flower-like, urchin-like and pine-needle-like, nanoparticles, nanowires, nano-honeycombs and nanothorns, have been studied extensively, while the supercapacitive performance of Ni ferrite ($NiFe_2O_4$) has been least studied [22]. In comparison to $NiCo_2O_4$, the synthesis of $NiFe_2O_4$ is cheaper and more environmental friendly because of natural abundance of iron and its less toxic nature. However, due to prominent agglomeration and low specific surface area of active sites, the $NiFe_2O_4$ exhibit poor specific capacitances [23]-[25]. Therefore, to improve the specific capacitance, it is worthy to synthesize good quality stable NiFe2O4 with high surface area of active sites.

With above view, in the present study, we have synthesized pure stable mesoporous $NiFe_2O_4$ nanoparticle via one step hydrothermal method and its capacitive behavior has been evaluated in 2 MKOH electrolyte by CV, GCD and EIS measurements in a three electrodes cell.

To the best of our knowledge, in this study, we are reporting the highest specific capacitance (~1040 $F.g^{-1}$ at 1 $A.g^{-1}$) for pure mesoporous $NiFe_2O_4$ nanoparticle on Ni foam substrate in 2M KOH electrolyte at room temperature. The synthesized material has been characterized by using XRD, TGA, TEM, FE-SEM and BET analysis.

Manuscript received October 19, 2016; revised May 26, 2017.

Nagesh Kumar, Amit Kumar, Sridhar Chandrasekaran and Tseung Yuen Tseng are with National Chiao Tung University, Taiwan (e-mail: nageshkumariitr@gmail.com; saini.14march@gmail.com; Sridharc9020@gmail.com; tseng@cc.nctu.edu.tw).

doi: 10.18178/jocet.2018.6.1.435

II. Experimental

A. Preparation of Spinel Nickel Magnetite

Well known hydrothermal approach was followed to synthesize spinel mesoporous FMO ($NiFe_2O_4$) nanoparticles. First, 0.606 g of iron nitrate, $Fe(NO_3)_3.9H_2O$ (Alfa Aesar), was dissolved in 37 mL of D.I water under continuous stirring. After that, 0.218 gm of nickel nitrate, $Ni(NO_3)_2.6H_2O$ (Alfa Aesar), and 0.526 gm of hexamethylenetetramine (HMT) were added into the above yellowish iron nitrate solution and kept stirring further for 2 h. The reddish-yellow homogeneous resultant solution was transferred into a 50 mL Teflon-lined sealed stainless steel autoclave. The reaction temperature was maintained at 120 °C for 8 h. After hydrothermal reaction, the material was mixed with 1.0 L D.I water and collected via vacuum filtration over nylon membrane filter paper, pore size 0.45 μm, diameter 47 mm. The final product was dried in an oven at 100 °C for 8 h.

B. Characterization

The prepared NFO nanoparticles powder sample was structurally characterized by X-ray diffractometer ((XRD, Bede D2)) employing CuKα (0.15406 nm) radiation and field-emission transmission electron microscope (FE-TEM, JEOL JEM-2100F). The surface morphology was examined by field emission scanning electron microscope (FE-SEM, Hitachi SU8010). To know the thermal stability of the FMO nanoparticles, thermal-gravimetric analysis (TGA) was performed from 50 to 800 °C at 5 °C min^{-1} ramping rate under N_2 environment using thermo-gravimetric analyzer (TGA, TA Instruments Q500). The specific surface area, pore volume and pore size distribution of the nanocomposite sample were determined by Brunauer-Emmet-Teller (BET) method (BET, ASAP 2020). For the surface area measurement, the sample (100 mg) was degassed for 8 h at 150 °C under N_2 flow (40 mL/min).

C. Electrode Preparation and Electrochemical Characterization

For the electrochemical performance of mesoporous NFO nanoparticles was evaluated in a three electrode configurations, where NFO nanoparticles powder works as working electrode, platinum sheet as counter electrode and a saturated calomel electrode (SCE) as reference electrode. Fresh 2 M KOH aqueous solution, prepared in D.I water, was utilized as an electrolyte. For working electrode fabrication, a consistent slurry was prepared by mixing NFO powder, super-P (conducting carbon) and PVDF (binder) in the ratio of 75:15:10 wt%. First, 10 mg PVDF was allowed to dissolve in an appropriate amount of NMP solvent via stirring and after that a well ground mixture of 75 mg NFO and 15 mg super-P was added into it. The final mixture was allowed to stirrer for 10 h. The obtained homogeneous slurry was applied uniformly on 1.0 cm^2 area of Ni foam substrate and then dried in a vacuum oven at 70°C for ~10 h. Before use, possible NiO layer on Ni foam substrate was removed by etching it in 3 M HCl solution for 30 min. The cyclic voltammetry (CV) measurements were performed between -0.1 and 0.45 V (vs. SCE) at different scan rates and the galvanostatic charge–discharge (GCD) tests were conducted from 1 to 15 Ag^{-1} in the potential window of -0.1 to 0.4 V (vs. SCE). The electrochemical impedance spectroscopy measurements were carried out in the frequency range from 100 kHz to 0.1 Hz at the open circuit potential with an AC amplitude of 5 mV. The specific capacitance (Fg^{-1}) from the CV curve was calculated based the following equation:

$$C = \frac{\int_{Ei}^{Ef} I(E)dE}{m.v.\Delta V} \quad (1)$$

where, *Ei* and *Ef* are the initial and final voltages in the CV curve analysis, ΔV is the potential window width, *I(E)* is the oxidation and reduction current (in amperes), *m* is the weight of the active electrode material and *v* is the scan rate.

The following equation was used to calculate the specific capacitance (Fg^{-1}) from GCD curve:

$$C = \frac{I.\Delta t}{\Delta V.m} \quad (2)$$

where, *I* is the discharging current (A), Δt is the discharging time, ΔV is the discharging voltage and m is the mass of active material.

All the electrochemical measurements were performed using Autolab PGSTAT128N electrochemical test system (Metrohm Auto lab B.V. Netherlands). Here, weight of the active material on the Ni foam substrate, as measured by the microbalance (PRECISA XR125SM-FR) with an accuracy of 0.1 μg, was ~ 0.7 mg.

III. Results and Discussion

A. Compositional and Morphological Studies

Fig. 1(a) represents the XRD pattern of NFO nanoparticles powder sample. It reveals the successful synthesis of pure-phase spinel NFO without any extra peaks of unreacted constituents or metal hydroxides. The diffraction peaks in this pattern at 2θ values of 18.4°, 30.3°, 35.7°, 43.2°, 53.8°, 57.4°, 63.2° and 74.6° are representative of (111), (220), (311), (400), (422), (511), (440) and (533) planes of the face centered cubic phase (space group $Fd\bar{3}m$) of NFO (JCPDS No. 42-1467). The existence of broad peaks in the XRD pattern suggest the presence of nanostructures in the sample.

The crystallite size (t) of NFO sample was calculated using Debye–Scherrer formula (eq. 3) and XRD peak of (400)

$$t = \frac{0.9\lambda}{\beta \cos\theta} \quad (3)$$

where β represents the full width at half maximum (FWHM) of X-ray peak in radians, λ is the wavelength (0.15406 nm for Cu Kα radiation) of the X-ray used. The calculated value of the crystallite size (t) comes out to be approximately 15 nm.

The thermal stability of the synthesized mesoporous NFO nanoparticles was studied using TGA. Fig. 1(b) is the TGA thermogram of the sample recorded in N_2 environment at a ramp rate of 5 °C min^{-1} in the range of 50 – 800 °C. Initial

3.8% weight loss of the sample occurred between 50 – 250 °C and it is attributed to the loss of moisture and to the removal of interlayered water molecules from the sample. A very small 2.5 % weight loss from 250 to 450 °C can be ascribed to the decomposition of residue precursor and to the improvement of crystallinity. No significant weight loss was absorbed as the sample heated further above 450 °C.

Fig. 1(c) and (d) demonstrates the pore size distribution curve and a typical N_2 adsorption–desorption isotherm of the NFO sample, respectively. Here we observe a broad mesopore size distribution in the range of 2–15 nm, with dominant pore size of 2 to 4 nm as shown in the inset of Fig. 1(c). So we conclude that in this sample porous structure is disordered. Fig. 1(d) shows that the adsorption isotherm at relative pressure (P/P0) from 0.4 to 1.0 is IV-type with a type H2 hysteresis loop (IUPAC). The existence of noticeable hysteresis loop in the isotherm is ascribed to the presence of mesopore among NFO nanoparticles. The analysis of nitrogen sorption results impart that NFO possesses BET surface area equal to 148 m^2g^{-1}, which is significantly higher than several previously reported results for pure NFO nanoparticles [20], [23]-[25]. The single-point adsorption total volume of pores at P/P0 = 0.9938 is 0.205 $cm^3\ g^{-1}$. These results suggest that our synthesized NFO sample possesses a loose mesoporous structure.

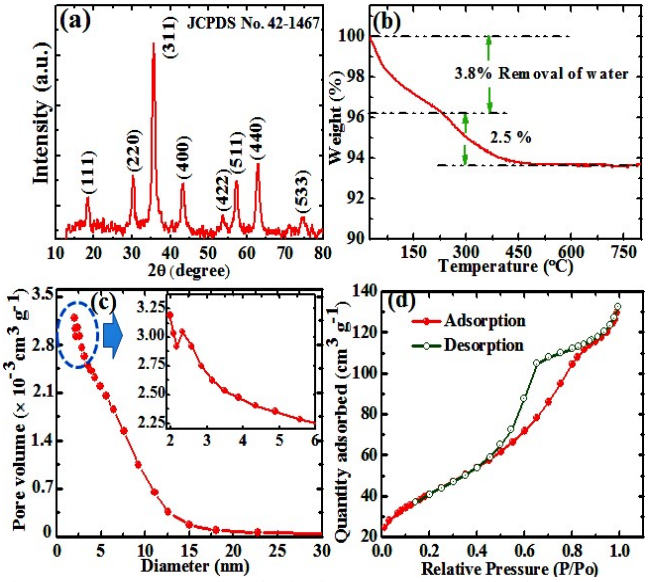

Fig. 1(a). XRD spectra of synthesized NFO powder sample, (b). TGA curve of NFO sample recorded in N2 environment at ramp rate of 5°C min-1, (c). The pore size distribution curve of the NFO and inset shows the magnified image of circled region, and (d). N2 adsorption–desorption isotherm.

Fig. 2 (a) represents the field-emission SEM (FESEM) images of the NFO nanoparticles. It shows that most of the nanoparticles are uniform in size and some of them are agglomerated. Fig. 2 (b) is the energy-dispersive X-ray spectroscopy (EDX) profile of NFO powder sample measured over a physical area shown in Fig. 2(a). In EDX profile, the x axis is the energy (keV) and the y axis represents the counts in arbitrary units. The EDX profile depicts the presence of Ni, Fe and O peaks, and there is no any impurity peak in the profile. The qualitative analysis of the Ni, Fe and O in the sample as estimated by EDX analysis, is shown in the inset of Fig. 2(b). The TEM image of the NFO powder sample (Fig. 2(c)) is in good agreement with our SEM results. Fig. 2(d) is the HRTEM image of the sample. It reveals the crystalline nature of the sample and the observed d-spacing values of ~0.209 and 0.295 nm are corresponding to (400) and (220) planes of cubic phase of spinal FMO. The TEM results are in good agreement with the XRD analysis.

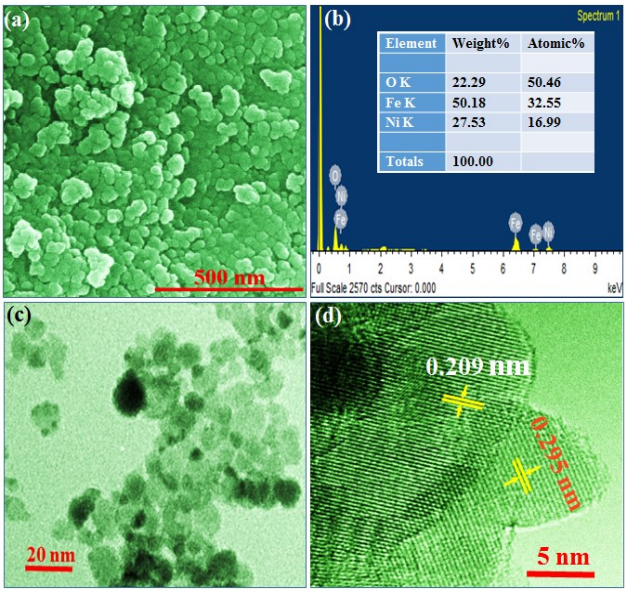

Fig. 2(a). FESEM images of NFO nanoparticles powder samples, (b). EDX spectrum of a small physical area and inset shows the elemental composition of the NFO sample as determined by EDX analysis, (c). TEM micrograph of a continuous and wrinkled rGO nanosheet and (d) HRTEM image of NFO nanoparticles.

B. Electrochemical Properties

The electrochemical behavior of mesoporous NFO nanoparticles on Ni foam substrate has been probed through CV, GCD and electrical impedance spectroscopy (EIS) measurements in 2 M KOH electrolyte at room temperature. Fig. 3 (a) shows the CV curves of the sample recorded at different scan rates of 5, 10, 15, 25, 50, 75 and 100 mVs^{-1}. We observe sharp redox peaks in all the CV curves, which correspond to the reversible redox (charge transfer) reactions occurring on the surface of the NFO nanoparticles. It implies that in our sample faradic charge storage mechanism is predominant. It can be noticed, with increase in the scan rate the cathodic and the anodic peaks in the CV curves shift in the direction of +ve and –ve potential regions, respectively. This peak shifting can be ascribed to the electrochemical polarization and it depicts the quasi-reversibility feature of the electrochemical redox reactions in the sample [26]. Fig. 3(b) represents the GCD behavior of the sample electrode at various current density values. Alike CV results, the GCD outcome also justifies the faradic nature of the sample electrode. The specific capacitances, measured from GCD data analysis using equation (2), at current density values of 1, 2, 3, 5, 7, 10, and 15 Ag^{-1} come out to be 1040, 920, 822, 700, 632, 638, 570 and 525 Fg^{-1}, respectively as shown in the inset of Fig. 3(b).

The measured specific capacitance 1040 Fg^{-1} at a current density of 1 Ag^{-1} for pure NFO sample is higher than several previously reported results [20], [23]-[25]. This excellent specific capacitance of NFO can be attributed to the mesoporous structure and its high specific surface area. Fig. 3

(c) represents the long cyclic stability performance of the sample at a current density of $2Ag^{-1}$. It is observed that system can maintain ~70 % of initial capacitance value after 500 charge/discharge cycles and this depletion in the capacitance value might be attributed to strong faradic reaction occurred at the material surface during electrochemical measurements. Fig. 3(d) represents the Nyquist plot of NFO samples as measured via electrochemical impedance spectroscopy (EIS) in the frequency range of 100 kHz to 0.1 Hz with AC amplitude of 10 mV. It depicts the characteristic features of the electron transportation between the electrolyte and the electrode surface. Nyquist plot exhibit a straight line in the low frequency region corresponding to the Warburg resistance caused by the frequency dependence of ion diffusion/transport from the electrolyte to the electrode surface. Determined from the point of intersection of the real axis in the range of high frequency, the internal resistance (R_1) is about 0.892 Ω. All spectra show a miserable semicircle from the high-frequency end to the middle-frequency region, attributed to the charge transfer resistance (R_2 = 223.3 m Ω) and double-layer capacitance at the electrode/electrolyte interface. The linear parts at lower frequencies correspond to the Warburg impedance (4.983×10^{-2}), which is defined as a diffusive resistance of the OH^- ion within the porous electrode. The low-frequency end shows capacitive-like behavior. This pattern of the impedance spectra to represent equivalent circuit is shown in the inset of Fig. 3(d). From the Nyquist data and the value of electrolyte resistance it is clear that NFO electrode has low charge transfer resistance.

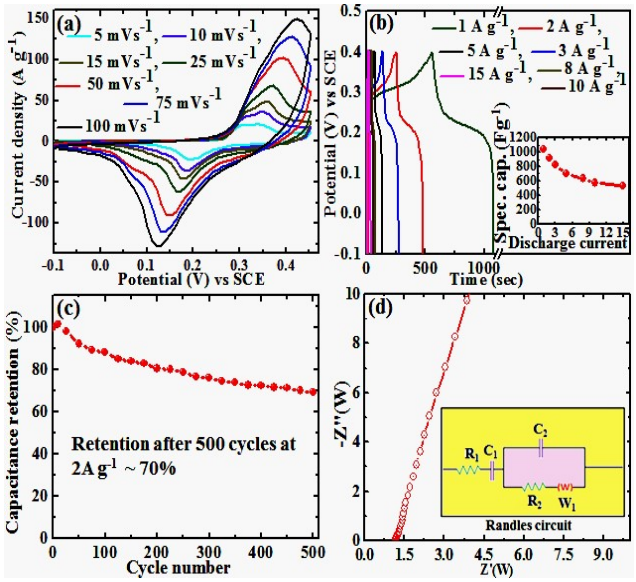

Fig. 3. Electrochemical studies of mesoporous NFO nanoparticles in 2 M KOH (a). CV curves at different scan rates of 5 to 100 mVs-1, (b). GCD curves at variable current densities from 1 to 15 Ag-1 and inset shows the specific capacitance calculated from GCD curves, (c). cycling stability by GCD curve at a current density of 2 Ag-1, and (d). Nyquist plots and inset shows the Randles circuit diagram.

IV. Conclusions

We have synthesized a pure cubic phase spinal mesoporous $NiFe_2O_4$ nanoparticles at low temperature (120 °C) via one step hydrothermal approach. The XRD, TEM, TGA and FE-SEM analysis verify the successful synthesis of cubic phase $NiFe_2O_4$ nanoparticles. BET measurements show that such synthesized $NiFe_2O_4$ nanoparticle powder possesses high surface area (148 m^2g^{-1}). The electro- chemical performance of $NiFe_2O_4$ nanoparticle on Ni foam substrate in 2 M KOH electrolyte in three electrodes system has been evaluated. $NiFe_2O_4$ nanoparticle electrode (active mass = 0.7 mg) exhibits very good specific capacitance (1040 Fg^{-1} at 1 Ag^{-1}) and ~ 70% retention after 500 cycles at 2 Ag^{-1}. These results indicate that our synthesized pure phase mesoporous $NiFe_2O_4$ nanoparticle is appropriate for the development of practical supercapacitor applications.

Acknowledgment

The authors are thankful to Prof. Ruey-an doong (nctu) for granting us permission to do electrochemical measurements in his laboratory

References

[1] T. R. Cook, D. K. Dogutan, S. Y. Reece, Y. Surendranath, T. S. Teeth, and D. G. Nocera, "Solar energy supply and storage for the legacy and nonlegacy worlds," *Chem. Rev.*, vol. 110, no. 11, pp. 6474-502, 2010.

[2] A. Chauhan, and R. P. Saini, "A review on integrated renewable energy system based power generation for stand-alone applications: configurations, storage options, sizing methodologies and control," *Renewable Sustainable Energy Rev.*, vol. 38, pp. 99-120, 2014.

[3] H. Jiang, P. S. Lee, and C. Li, "3D carbon based nanostructures for advanced supercapacitors," *Energy Environ. Sci*., vol. 6, pp. 41-53, 2013.

[4] P. Simon, and Y. Gogotsi, "Materials for electrochemical capacitors," *Nat. Mater*., vol. 7, pp. 845-854, 2008.

[5] A. G. Pandolfo and A. F. Hollenkamp, "Carbon properties and their role in supercapacitors," *J. Power Sources*, vol. 157, pp. 11-27, 2006.

[6] X. Lang, A. Hirata, T. Fujita, and M. Chen, "Nanoporous metal/oxide hybrid electrodes for electrochemical supercapacitors," *Nat. Nanotechnol*., vol. 6, pp. 232-236, 2011.

[7] H. Wei, J. Zhu, S. Wu, S. Wei, and Z. Guo, "Electrochromic polyaniline/graphite oxide nanocomposites with endured electrochemical energy storage," *Polymer*, vol. 54, pp. 1820-1831, 2013.

[8] Z. Li, Z. Zhou, G. Yun, K. Shi, X. Lv, and B. Yang, "High-performance solid-state supercapacitors based on graphene-ZnO hybrid nanocomposites," *Nanoscale Res. Lett*., vol. 8, no. 1, p. 473, 2013.

[9] Z. Fan, J. Yan, T. Wei, L. Zhi, G. Ning, T. Li, and F. Wei, "Asymmetric supercapacitors based on graphene/MnO_2 and activated carbon nanofiber electrodes with high power and energy density," *Adv. Funct. Mater.*, vol. 21, pp. 2366-2375, 2011.

[10] C. Yuan, X. Zhang, L. Su, B. Gao, and L. Shen, "Facile synthesis and self-assembly of hierarchical porous NiO nano/micro spherical superstructures for high performance supercapacitors," *J. Mater. Chem.*, vol. 19, pp. 5772-5777, 2009.

[11] T. W. Lin, C. S. Dai, and K. C. Hung, "High energy density asymmetric supercapacitor based on NiOOH/Ni_3S_2/3D graphene and Fe_3O_4/graphene composite electrodes," *Sci Rep.*, vol. 4, p. 7274, 2014.

[12] Z. Chen, V. Augustyn, J. Wen, Y. Zhang, M. Shen, B. Dunn, and Y. Lu, "High-performance supercapacitors based on intertwined CNT/V_2O_5 nanowire nanocomposites," *Adv Mater*., vol. 23, pp. 791-795, 2011.

[13] C. C. Hu, K. H. Chang, M. C. Lin, and Y. T. Wu, "Design and tailoring of the nanotubular arrayed architecture of hydrous RuO_2 for next generation supercapacitors," *Nano Lett*., vol. 6, pp. 2690-2695, 2006.

[14] N. Kumar, C. W. Huang, P. J. Yen, W.-W. Wu, K.-H. Wei, and T. Y. Tseng, "Probing the electrochemical properties of an electrophoretically deposited Co_3O_4/rGO/CNTs nanocomposite for supercapacitor applications," *RSC Adv*., vol. 6, pp. 60578-60586, 2016.

[15] S. Sahoo, K. K. Naik, and C. S. Rout, "Electrodeposition of spinel $MnCo_2O_4$ nanosheets for supercapacitor applications," *Nanotechnology*, vol. 26, pp. 1-8, 2015.

[16] S. Sun, S. Li, S. Wang, Y. Li, L. Han, H. Kong, and P. Wang, "Fabrication of hollow $NiCo_2O_4$ nanoparticle/graphene composite for supercapacitor electrode," *Mater. Lett*., vol. 182, pp. 23-26, 2016.

[17] G. K. Veerasubramani, K. Krishnamoorthy, S. Radhakrishnan, N. J. Kim, and S. J. Kim "Synthesis, characterization, and electrochemical properties of $CoMoO_4$ nanostructures," *Int. J. Hydrogen Energ*., vol. 39, pp. 5186–5193, 2014.
[18] K. V. Sankar, R. K. Selvan and D. Meyrick, "Electrochemical performances of $CoFe_2O_4$ nanoparticles and a rGO based asymmetric supercapacitor," *RSC Adv.*, vol. 5, pp. 99959–99967, 2015.
[19] H. Yan, T. Li, K. Qiu, Y. Lu, J. Cheng, Y. Liu, J. Xu, Y. Luo, "Growth and electrochemical performance of porous $NiMn_2O_4$ nanosheets with high specific surface areas," *J. Solid State Electr*., vol. 15, pp. 3169–3175, 2015.
[20] V. Venkatachalam and R. Jayavel, "Novel synthesis of Ni-ferrite ($NiFe_2O_4$) electrode material for supercapacitor applications," *AIP Conf. Proc*., vol. 1665, p. 140016, 2015.
[21] N. Guo, X. Q. Wei, X. L. Deng, and X. J. Xu, "Synthesis and property of spinel porous ZnMn2O4 microspheres," *Appl. Surf. Sci.*, vol. 356, pp. 1127–1134, 2015.
[22] Z. Wu, Y. Zhu, and X. Ji, "$NiCo_2O_4$-based materials for electro chemical supercapacitors," *J. Mater. Chem. A*, vol. 2, pp. 14759–14772, 2014.
[23] P. Sen and A. De, "Electrochemical performances of poly (3,4-ethylene dioxythiophene)–$NiFe_2O_4$ nanocomposite as electrode for supercapacitor," *Electrochim. Acta*, vol. 55, no. 16, pp. 4677–4684, 2010.
[24] Z. Wang, X. Zhang, Y. Li, Z. Liu, and Z. Hao, "Synthesis of graphene –$NiFe_2O_4$ nanocomposites and their electrochemical capacitive behavior," *J. Mater. Chem. A*, vol. 1, pp. 6393–6399, 2013.
[25] S.Anwar, K. S. Muthu, V. Ganesh, and N. Lakshminarasimhan, "A comparative study of electrochemical capacitive behavior of $NiFe_2O_4$ synthesized by different routes," *J. Electrochem. Soc*., vol. 158, no. 8, 2011.
[26] L. B. Kong, J. W. Lang, M. Liu, Y. C. Luo, and L. Kang, "Facile approach to prepare loose-packed cobalt hydroxide nano-flakes materials for electrochemical capacitors," *J. Power Sources*, vol. 194, no. 2, p. 11941201, 2009.

Nagesh Kumar was born at Saharanpur city in India. He received his Ph.D. degree from Department of Physics and Centre for Nanotechnology, Indian Institute of Technology Roorkee, India in 2014. Currently he is a postdoc fellow in National Chiao-Tung University, Hsinchu, Taiwan and doing his research work under the supervision of Prof. Tseung-Yuen Tseng. His research areas of interest are gas sensors, 1-D, 2-D materials and energy storage devices (supercapacitors, Li-ion batteries).

Amit Kumar was born in Meerut City, India, in 1986. He received his M.S. From Chaudhary Charan Singh University, Meerut City, India in 2011 and then joined the Indian Institute of Technology (I.I.T) Kharagpur, India in Materials Science as a Project Assistant to 2012. Now he is a Ph.D. candidate under the super- vision of Prof. Tseung-Yuen Tseng and Prof. Jihperng Leu. His research interest focuses on energy and Supercapacitors.

Sridhar Chandrasekaran was bron in Chennai, India in 1990. He received his M.Tech degree in VLSI design from SRM University. India, in 2014. He is currently pursuing his Ph.D. degree with the EECS International Graduate Program, National Chiao Tung University, Hsinchu, Taiwan. He is also involved in the fabrication and characterization of resistive switching memory devices under the supervision of Prof. Tseung-Yuen Tseng.

Tseung-Yuen Tseng was born in Hong Kong in January 8, 1953. He received his Ph.D. degree in electroceramics from the School of Materials Engineering, Purdue University, West Lafayette, USA in 1982.

He was briefly associated with the University of Florida, Gainesville, before joining National Chiao-Tung University, Hsinchu, Taiwan in 1983, where he is now a University Chair Professor in the Department of Electronics Engineering and the Institute of Electronics. His professional interests are science and engineering of electronic nanoceramics materials and devices, ferroelectric thin films based devices, high-k dielectric films, resistive switching memory devices, passive components based metal electroded multilayer capacitors, varistors, PTCR, ceramic sensors, high temperature superconducting ceramics, structure-composition-property relationships, Nanoceramics, nanopowders, nanocomposites, nanotubes, nanowires and field emission devices, ceramic sensors and supercapacitors.

Prof. T.-Y. Tseng was the Vice Chancellor and University Chair Professor of the National Taipei University of Technology, Taipei, Taiwan (2007-2009). He is Editorial Board Member of Advances in Ceramic Science and Engineering (2012-present) also Associate Editor of Advanced Science Letters(2007-2012), and Journal of Nanoscience and Nanotechnology(2005-present). He published more than 350 research papers and more than 30 patents. He wrote more than 7 scientific books.